APPENDIX G

EVALUATION OF REACTOR PRESSURE VESSEL (RPV) NOZZLE TO HOT-LEG PIPING BIMETALLIC WELD JOINT INTEGRITY FOR THE V. C. SUMMER NUCLEAR POWER PLANT

G.1 SUMMARY

In October 2000 the V. C. Summer Plant was shut down for a normal refueling outage. During the normal inspection a leak was discovered in the vicinity of one of the reactor pressure vessel (RPV) outlet nozzle to hot-leg pipe bimetallic welds. Ultrasonic tests performed on the pipe from the inside surface revealed a single axial flaw near the top of the pipe. During destructive inspection of the crack zone, additional smaller axial flaws were identified, along with several small circumferential indications. The cracking was attributed to primary water stress corrosion cracking (PWSCC).

In order to be able to predict the growth rates for these PWSCC cracks, and therefore, predict the amount of time required before leakage occurs, a detailed analytical model of the V. C. Summer bimetallic pipe weld was performed. All of the fabrication processes involved in the construction and repair of the V. C. Summer hot leg bimetal weld were considered. This included hot leg buttering and welding of a pressure vessel nozzle to a stainless steel pipe using Inconel 82/182 filler material, material removal and repair, heat treatment, and service loads. PWSCC crack growth predictions were made for the cases of weld residual stresses only, and residual stresses with service loads. Predictions of axial cracks growth rates along with circumferential crack growth rates were made. Some of the key results from this series of analyses are summarized in the following paragraphs.

For reducing the effect of both axial and circumferential PWSCC after weld repairs, inside welding followed by outside welding is preferred. Both cases were considered in the analyses since the precise repair sequence in the V. C. Summer plant was not known. This illustrates the power of computational weld models and suggests that field weld repairs should be designed and driven by a corresponding weld analysis to reduce the propensity for SCC in piping.

In particular, hoop residual stresses (which lead to axial cracking) after complete fabrication are mostly tensile in the weld region. For the case of outside weld repair followed by inside welding, high tensile residual stresses are produced everywhere. For the inside weld followed by outside weld case, a small zone of compressive hoop residual stresses develop at the pipe inside surface at the weld. Moreover, hydro testing does not alter fabrication residual stresses very much.

Service load effects on PWSCC were also considered. Heating the hot leg pipe system up to operation temperature of 324°C (615°F) actually reduces axial fabrication stresses to mainly compressive values due to the expansion of the hot leg pipe and the rigid constraint provided by the vessel and steam generator. Hoop residual stresses are unaffected by heating up to operating temperatures. Since as fabricated axial residual stresses are low at operating temperature, circumferential stress corrosion cracking is not expected due solely to fabrication stresses. Service loads dominate circumferential PWSCC.

Axial crack growth is dominated by fabrication residual stresses, but the internal pressure does play an important role in PWSCC. Weld repairs can alter residual stresses in pipe fabrications. In general, stress reversal in sign occurs near the start/stop locations of the repair. This can possibly result in a PWSCC crack stopper or can slow down the crack growth rate as the crack approached these locations. A similar reversal in the sign of the stress occurs in a baseline weld near the torch start/stop locations or weld repairs.

The analysis results here show that axial cracking should be confined to the weld region. Starting from a crack 5 mm (0.2 inches) in depth, the crack should break through the pipe wall within two years. The crack nucleation time is something that should be studied in more detail in the future. Circumferential cracks should take about twice as long to become a through wall crack compared with axial cracks. Circumferential cracks will tend to grow longer than axial cracks. However, since service loads dominate circumferential cracks, they will slow their circumferential growth as they grow toward the bottom of the pipe. Here, by bottom of the pipe,

it is understood to be the compressive bending stress region of the pipe. The service loads consist of thermal expansion mismatch, tension caused by 'end cap' pressure, and bending. The bending stresses caused by a bending moment are compressive 180 degrees from tension zone. Part through circumferential cracks that initiate in the tension zone and grow beyond the bending neutral axis may slow down as they approach the compressive bending stress zone. However, for non-fixed bending axes, where the tension zone changes, this may not be significant.

Grinding of welds may lead to scratches, which in turn may lead to crack initiation sites. Grinding of welds should be performed carefully. It is of use to study the effect of grinding on both residual stresses (caused by grinding) and crack initiation sites. Numerical models of the grinding process can and should be developed and used to guide field grinding operations.

Finally, PWSCC growth would be best considered using a risk based probabilistic approach using TRACLIFE or similar code because of the inherent variability in many factors that lead to corrosion cracking.

G.2 INTRODUCTION

In October 2000 the V. C. Summer Plant was shut down for a normal refueling outage. During the normal inspection, significant boron deposits were discovered in the vicinity of an RPV outlet nozzle to pipe weld for the hot leg pipe (large pipe from the reactor pressure vessel to the steam generator). Leakage records showed a nearly constant value of 0.3 GPM unidentified leakage from all sources, well below the plant technical specification limit of 1.0 GPM (Ref. G.1).

The design geometry of the nozzle to pipe weld is shown in Figure G.1. Ultrasonic tests performed on the pipe from the inside surface revealed a single axial flaw near the top of the pipe [Ref G.1]. The flawed region was then removed, and a new spool piece was welded in place. The repair weld was made with Alloy 52, a material which is much more resistant to SCC

(stress corrosion cracking) compared with Alloy 82/182.

The purpose of this study was to study the cracking behavior in bimetallic welds of the type used in the V. C. Summer plant. Tensile weld residual stresses, in addition to service loads, contribute to PWSCC (Primary Water SCC) crack growth. In order to be able to predict crack growth rates, and therefore, predict the amount of time required before leakage occurs for normal PWR conditions, a detailed analytical model of the V. C. Summer bimetallic pipe weld was performed.

The work plan outlined here was to help support the NRC's assessment of the cracking found in the 'A' RPV nozzle to hot-leg pipe bimetal weld in the Virgil C. Summer nuclear plant. The hot leg weld is a bimetallic weld joining a SA-508 (Class 2) reactor vessel nozzle with a Type 304N stainless steel pipe using an Inconel weld procedure (Figure G.1). Figure G.2 illustrates the geometry of this type of nuclear plant in simple format. The hot leg pipe carries reactor-heated water to the steam generator. It is then re-circulated by the pump back through the 'cold leg'. Both the hot and cold leg stainless steel pipes are joined to the reactor vessel nozzles via bimetallic welds. The cracking of concern occurs in the Inconel weld only.

The analysis work reported here was broken into three tasks. The first task was to model the residual stresses that develop from welding. This analysis included the effects of selected repair weld analyses. The second was to validate the model by performing measurements on a similar bimetallic welded pipe that was obtained during an earlier NRC program at Battelle (Ref. G.2). The final task involved evaluating stress intensity factors along with performing simple pressurized water stress corrosion cracking (PWSCC) analyses of the cracks. All work was performed as part of Task 8 of the BINP Program. Funding for this Task 8 activity was provided by the US NRC.
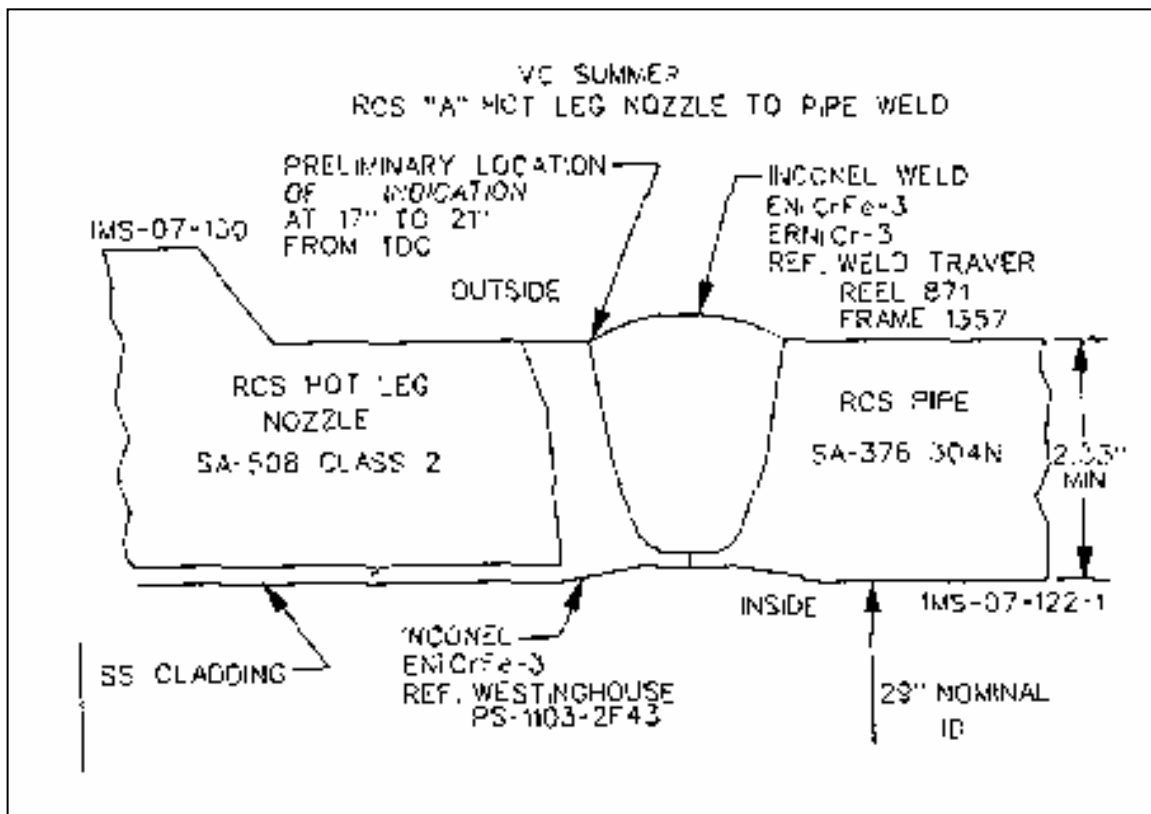
Figure G.1 Geometry of VC Summer hot leg/RPV nozzle bimetallic weld joint

G.3 GENERAL OVERVIEW OF ANALYSIS WORK PERFORMED

Three separate sets of weld analyses were performed. These included: (i) analysis of a cold leg bimetallic weld used in an experiment conducted by Battelle in an earlier NRC sponsored program [2], (ii) analysis of a typical design bimetallic weld in the V. C. Summer plant for V. C. Summer hot legs 'B' and 'C', and (iii) repair weld analyses of several typical repairs. The first analysis was planned for model validation purposes while (ii) was planned to predict the crack growth response within residual stress fields and operating loads for a typical hot leg plant weld. Analysis set (iii) quantified the important effect that weld repairs have on weld induced residual stresses

and on the corresponding crack growth through the repair weld residual stress fields.

The analyses in sets (i) and (ii) were performed using both axis-symmetric analysis and full 3D analysis. The analysis set (iii) was performed using full 3D analysis. It is noted that 3D welding considerations can have an important effect on the residual stresses, especially in the region of the weld start/stop locations and for considering the effects of weld repairs. The axis-symmetric analyses of (i) and (ii) provided an initial 'general' overview of the residual stress fields in this bimetallic weld. However, as discussed below, full 3D effects will be included in the fracture assessment even for the axis-symmetric weld modeling case.
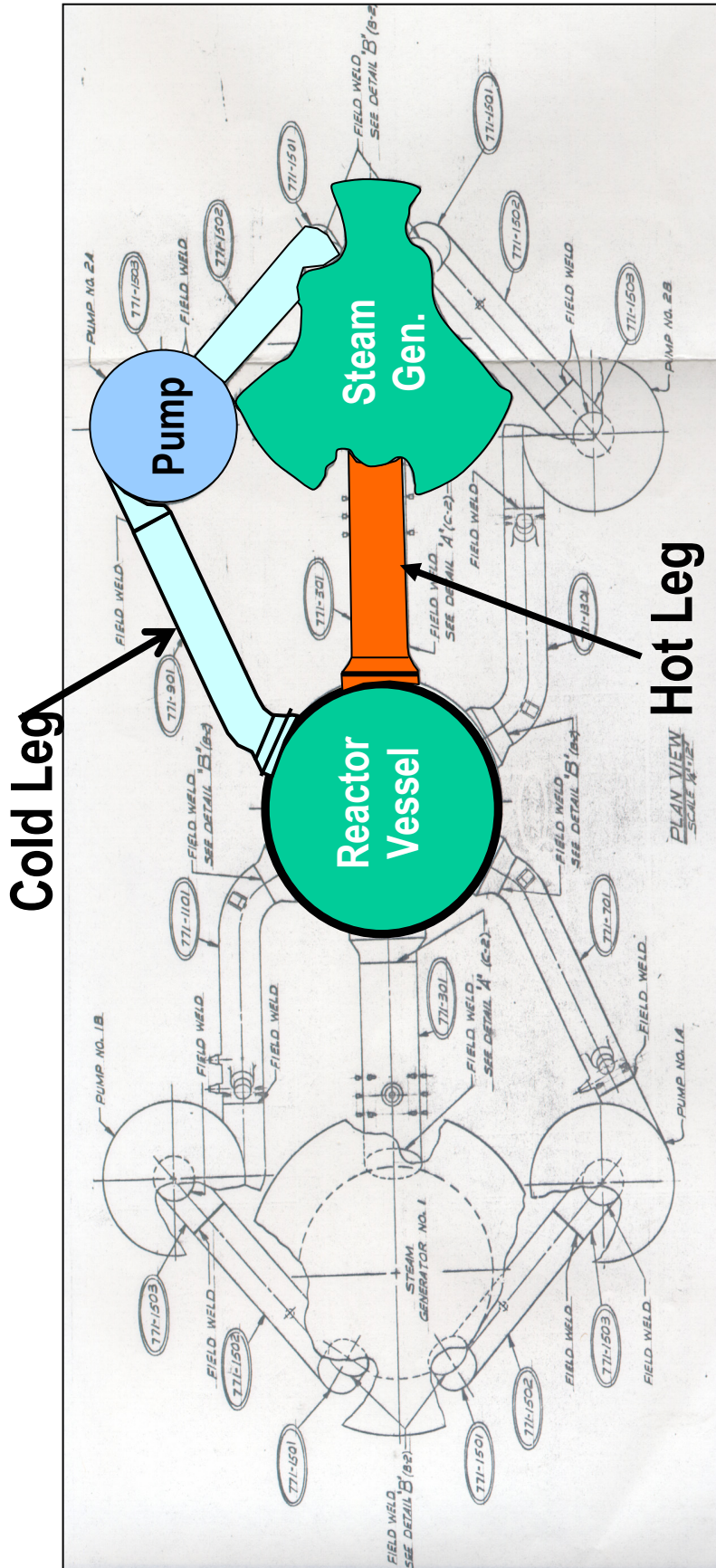
Figure G.2 Piping system geometry

G.3.1 Weld Residual Stress Analysis

The series of weld modeling analyses listed below were performed.

- **Axis-symmetric Cold Leg Analysis.** A weld analysis of a bimetallic weld from a cold leg that was tested as part of the NRC program 'Short Cracks in Piping and Piping Welds' program was performed first. The weld analyzed joined an A516 Grade 70 carbon steel pipe to a 316 SS safe end using an Inconel weld procedure (Figure G.3). The pipe diameter was 36-inch with a thickness of 3.4 inches. The materials and geometry of this case are similar to the hot and cold leg welds in the V. C. Summer plant. The purpose of this analysis was to validate the weld models for the bimetallic weld case. It should be noted that Battelle's weld models (VFT^{TM} [3]) have extensive validation from other programs in industry, US Government, and overseas utilities. It will be seen, however, that the residual stress measurements from this effort are of questionable validity.

- **Axis-symmetric Hot Leg Analysis.** Weld analysis of the design hot leg bimetallic welds in the V. C. Summer plant were conducted. This analysis was quite complicated since the actual field welds sequence; including grinding and repair were considered. This analysis predicted the residual stresses for use in a fracture assessment in Task 3. Weld joint specifications and material properties available from the licensee were provided by the NRC so as to accurately model the residual stresses.

- **Three Dimensional Analysis of Hot Leg.** The analyses discussed above assumed axis-symmetric conditions for the analysis. It is known that full three dimensional weld residual stress states can vary significantly from an axis-symmetric solution near the regions of the weld torch start/stop positions. In general, compressive residual stresses often develop near the regions of the start/stop locations. As such, an axis-symmetric solution is normally considered conservative compared with a full three dimensional solution. With this in mind, the three dimensional analysis of the hot leg weld was performed to quantify the '3-D' effects on PWSCC in PWRs. Two separate repair lengths and two depths (a total of three repair analyses) were performed. These consisted of a long and short length repair with a shallow depth, and a short length repair with a deeper depth. The repair solution procedure consists of first modeling the original bimetallic weld. This is a computationally intense solution since there are so many passes involved. Next, the material removal in preparation for the repair was modeled. Finally, the repair passes were modeled. For all repair cases, the predicted residual stresses were used to predict SCC crack growth.

Finally, all analyses were performed using the VFT^{TM}'s weld analysis code (Ref. G.3), which was developed jointly by Battelle and Caterpillar. This code has an extensive database of validation for complex welded structures and is considered to be the best available weld analysis code.

G.3.2 Weld Residual Stress Measurements

This task involved determining the residual stresses from the Battelle bimetallic test case to further validate the models for bimetallic welds. Battelle still has sections of the original pipes that were taken from a canceled plant. A trepanning technique was used to obtain surface measurements of the residual stresses.

G.3.3 Fracture Mechanics and PWSCC Analysis

Stress intensity factors were determined by first mapping the results obtained from the weld analyses to a full three-dimensional finite element model. The stress intensity factors were determined from the residual stress fields using the finite element alternating method (FEAM) code developed by Battelle (Ref. G.4). In addition, service loads were applied over top the residual stresses to obtain the loads for PWSCC analysis as well. FEAM is an extremely
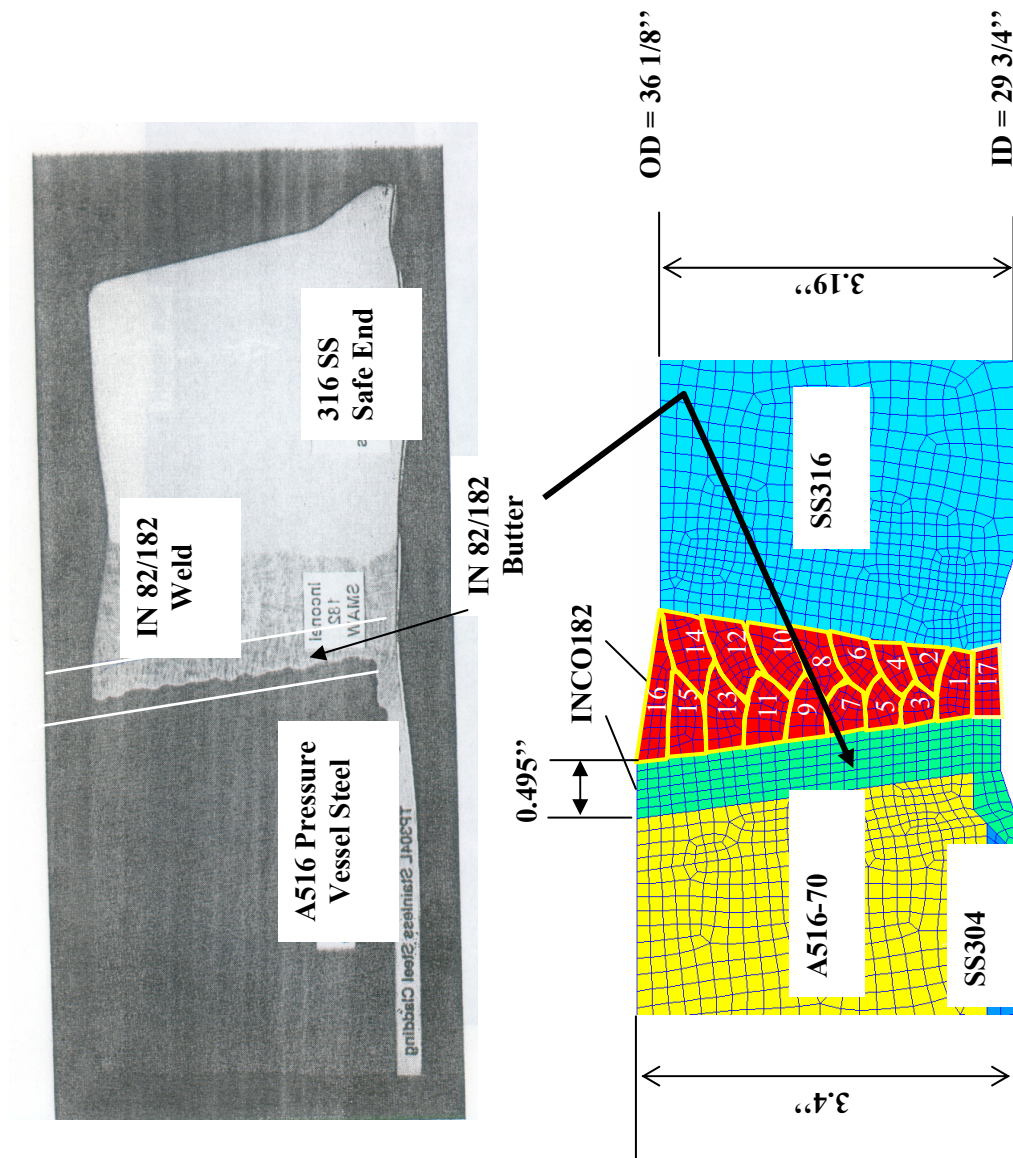
Figure G.3 Photo of cold leg weld cross section (top) and computational weld model of cold leg

efficient method for fracture analysis that was developed recently in the aerospace community and has FAA and Air Force acceptance. In addition, Battelle has been using FEAM for weld fracture analyses for Argonne National Laboratory (as part of another NRC program), as part of a DOE weld fracture analysis program for Savannah River, and for European utilities. It is accepted as accurate and has been extensively validated. The effect of weld residual stress redistribution during crack growth is accurately accounted for with FEAM. The efficiency of FEAM is because a special crack mesh is not needed – rather the mesh for the *uncracked* geometry is all that is required, and K solutions can be obtained for many crack sizes, shapes, and locations with this one mesh.

Both circumferential and axial crack solutions were obtained for both surface and through-wall cracks. From the recent documentation of the V. C. Summer cracking it is clear that both types of cracking have been observed. Flaw indications have been identified using ultrasonic testing (UT) and eddy current testing (ECT) in hot legs A, B, and C as reported in December 2000 and January 2001 licensee public meeting presentations. The stress intensity factor (K) was determined for about 20 cracks of various sizes and locations. It is emphasized that the full 3D analysis using ABAQUS is time consuming and costly compared with FEAM solutions.

Finally, PWSCC predictions were made using the K solution results. The analyses of PWSCC include the effect of residual stress redistribution caused by crack growth. The TRACLIFE code (Ref. G.5), originally developed for the FAA, was used to make the crack growth life predictions.

G.4 ANALYSIS TOOLS

From the discussion above, it is seen that three different analysis tools were used to perform these analyses. The analysis tools are:

1. VFT^{TM} – Virtual Fabrication Technology and Weld Modeling Code.

2. FRAC@ALT - Finite Element Alternating Method (FEAM) Code.

3. TRACLIFE – Probabilistic and Deterministic Life Prediction Code.

G.5 RESULTS COLD LEG ANALYSIS

As discussed above, the first step in the analysis of the hot leg PWSCC issue was to obtain confidence in the computational weld model. As discussed in Reference G.3, the VFT code used for the weld modeling analyses has an extensive validation data base library for same material welding (stresses and displacements). However, little data exists for bimetallic welds. As part of the validation of the analysis procedures for bimetallic welds, it was decided to perform a weld analysis of a cold leg pipe that Battelle had stored from the US NRC Short Cracks in Piping and Piping Welds program (Ref. G.2). This stored pipe then had its residual stresses measured using the classic trepanning technique (Ref. G.6). The predicted residual stresses were then compared with the measured stresses. Unfortunately, the measured stresses appeared to be quite low compared with what was expected. This is discussed later in this section.

G.5.1 Cold Leg Computational Weld Model

Figure G.3 illustrates the axis-symmetric weld model in the lower figure and a photograph of the weld cross-section for the bimetallic weld that was tested in the upper figure. It is seen that this section had an A516 Grade 70 pipe welded to a Type 316 stainless steel safe end pipe with Inconel 82/182 filler metal. Sixteen passes were required to complete the weld. This is a large diameter, thick pipe.

The analysis sequence flow chart is shown in Figure G.4 and graphically illustrated in Figure G.5. The A516 pipe was first machined and a 304 stainless steel cladding was applied to the inner surface. The weld deposition of the 304 stainless steel cladding layer was not modeled here. However, the material properties of the cladding were considered, i.e., a thin layer of 304 stainless steel material properties was
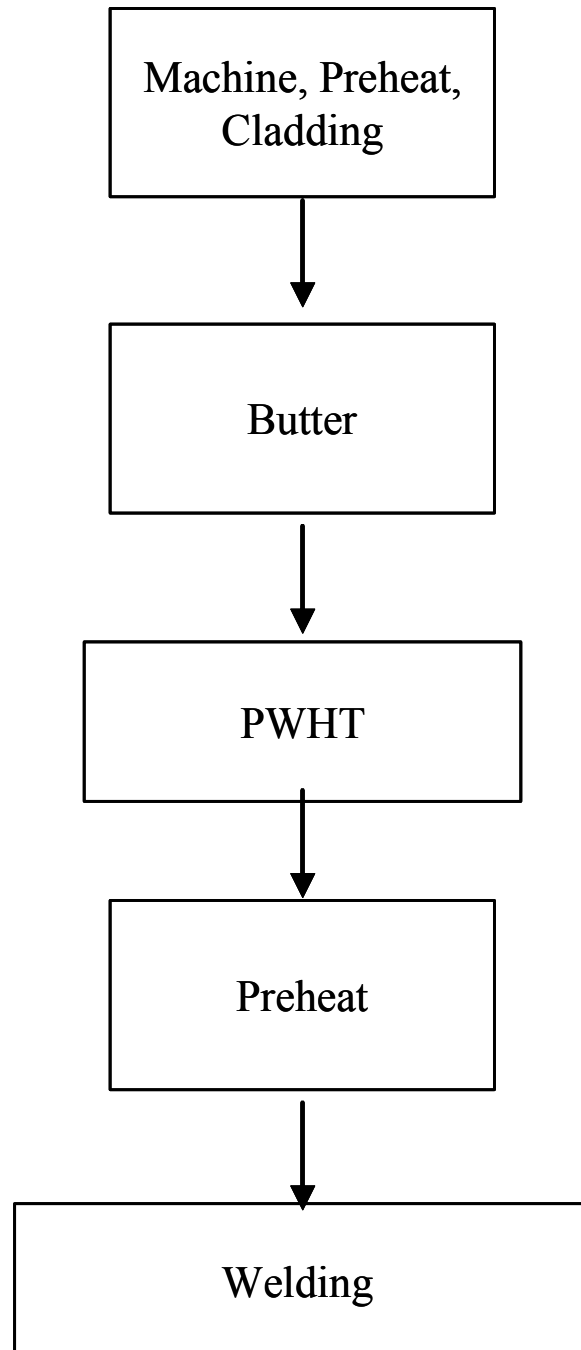
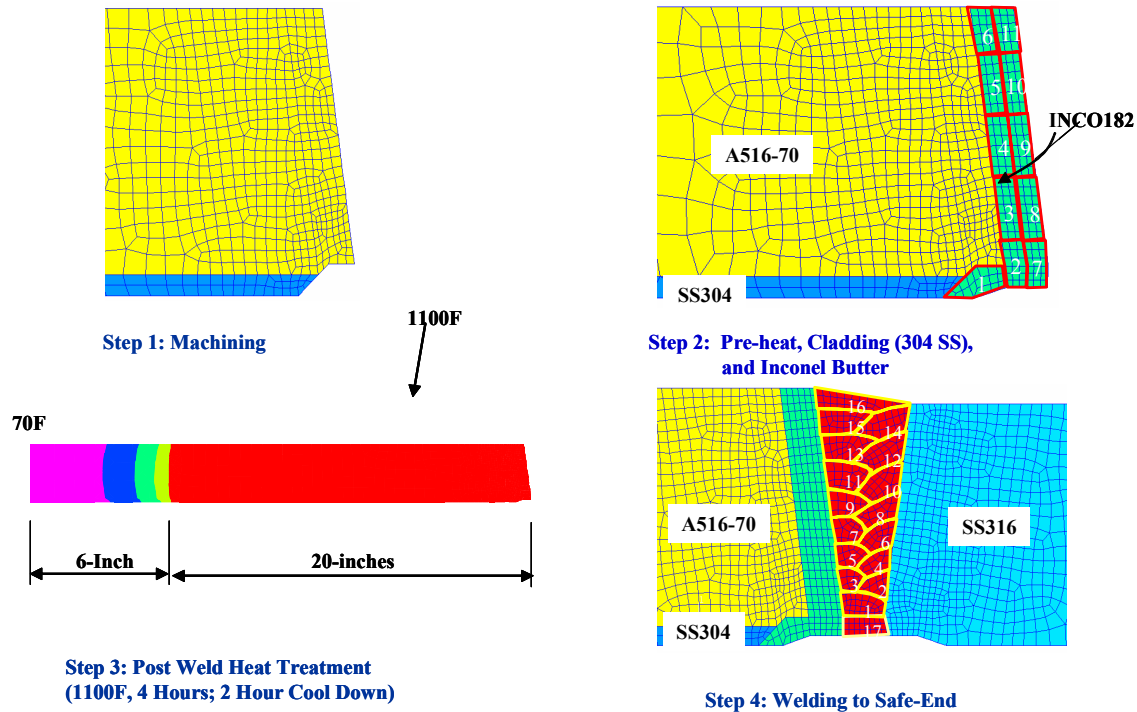**Figure G.4 Welding process analysis flow chart for cold leg**

Figure G.5 Cold leg axis-symmetric cladding (buttering) and weld model

used at this region so that the material property mismatch is included in the Inconel weld modeling steps. The weld cladding deposition step was not included here because cracking in the buttering and Inconel weld metal was of main concern in this analysis. The residual stresses from the buttering, PWHT, and butt weld deposition will tend to dominate residual stresses in the region of interest (weld and butter zone). In effect, the local cladding residual stresses are 'annealed' or 'stress relieved' by the buttering and later weld processes, and were thought to be of second order importance. Of course, such residual stresses are indeed important at regions away from the butt weld.

An Inconel buttering layer was then applied to the A516 pipe in preparation for the weld. From Figure G.5 it is seen that the buttering was deposited in 11 passes. The A516 pipe was then subjected to a post weld heat treat of 1100°F for four hours. The post weld heat treat was modeled by permitting the stresses to relax via creep. The weld metal was then deposited to complete the bimetallic weld. Again from Figure G.5, 16 passes were required. The buttering and weld sequence and weld pass sizes were

estimated from the weld paper work for the actual production weld, and from the photograph of the weld cross section.

Figure G.6 further illustrates the weld modeling process. It is also seen that the root pass was ground out after welding and re-deposited. It is not clear why this was done in the field, but the process of grinding and re-welding the root pass was included in the model.

In modeling the weld process, particularly for multi-pass welds, it is important to properly model the history annihilation (or local 'annealing') process. More details of this constitutive model can be found in References G.7 and G.8. It is important to note that without modeling this history annihilation process, unrealistic plastic strains develop in the model predictions that have a significant effect on the predicted residual stress state. Moreover, the solution times of the computational model are significantly increased. The constitutive law is a classical thermal elastic-plastic law with features which permit history annihilation, phase changes (not important here), large deformations, melting/re-melting, and accounts for 'not yet
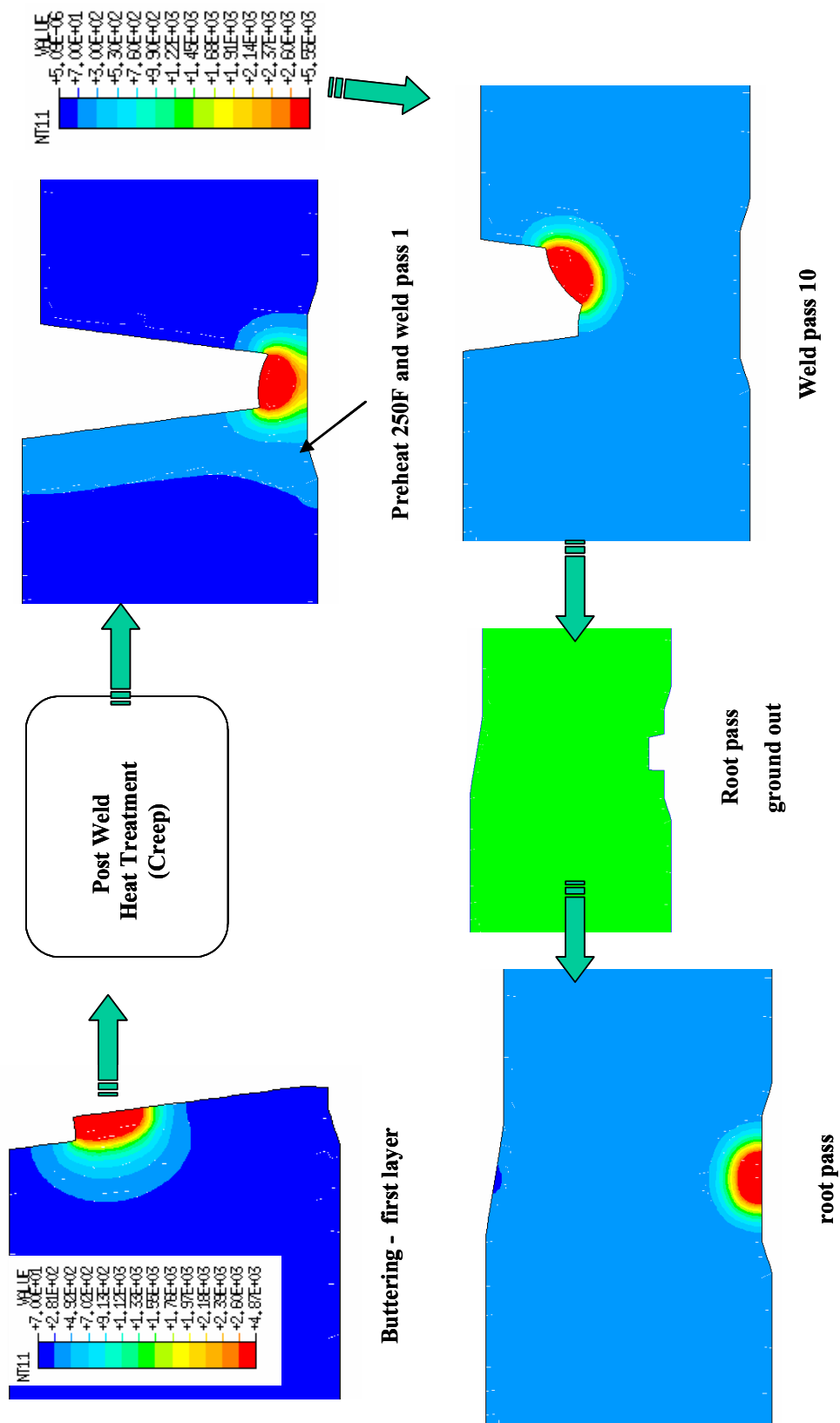
Figure G.6 Weld process simulation

deposited' weld metal in a computationally efficient manner using a concept called virtual element detection (Ref. G.8).

The material properties used for the thermal analysis for the Inconel 82/182 weld metal, the A516 Grade 70 pipe, and the 316 and 309 stainless steels are shown in Tables G.1 to G.5. Tables G.1 to G.5 also list elastic properties used in the constitutive modeling of the weld process. Figure G.7 illustrates the temperature dependent elastic plastic properties for the Inconel weld, A516 Grade 70 carbon steel pipe, and Type 316 stainless steel safe end used in the analyses. The tensile properties for Inconel 182 were obtained specifically for this program by Oak Ridge National Laboratory (ORNL). The elastic-plastic properties for the A516 Grade 70 pipe were obtained from the literature, and the stainless steel properties were obtained from prior work done at Battelle. It is important to note that the thermo-plastic properties used for a proper weld modeling analysis (for the weld material) should be stress relieved and annealed prior to testing since the weld modeling process itself models the work hardening process caused by the welding.

Finally, Table G.6 shows creep properties used to model stress relaxation during the post weld heat treatment. Note that at 1100F (the post weld heat treat temperature (PWHT)) the A516 Grade 70 steel experiences the most creep deformation. Moreover, note that the stainless steel (see Figure G.5) is not in the model yet for the PWHT.

G.5.2 Cold Leg Results After Butter and PWHT

Figure G.8 illustrates the axial residual stress state of the A516 pipe after buttering and PWHT is complete. (Note: all stresses in this report are in ksi units.) The analysis sequence begins in the upper left figure and proceeds clockwise. Note that by the time the PWHT is complete and cooling to room temperature occurs, the initial residual stress state has changed significantly. Likewise, the axis-symmetric hoop stresses through the PWHT process after buttering is shown in Figure G.9. It is clear the hoop

stresses are relaxed via PWHT more so the than axial stresses. Moreover, including the effect of the PWHT in the analysis process is important.

The equivalent plastic strains after buttering and after PWHT are shown in Figure G.10. It is noted that when modeling the PWHT process via a creep constitutive model, plasticity is included (i.e., a combined creep-plasticity model was used). It is seen that the creep relaxation process is mainly due to creep, with additional plasticity having a second order effect. Figure G.11 shows the effective creep strains that accumulate after the PWHT. The top illustration in Figure G.11 is of a large portion of the pipe. Notice the accumulation of creep strains near the end of the PWHT region (see Figure G.5 also). Other researchers have observed this as well when modeling the heat treat process. Notice from the bottom illustration of Figure G.11 that the largest tensile creep strains occur near the outer diameter of the A516 pipe adjacent to the Inconel butter.

G.5.3 Cold Leg Results After Completed Weld

The axial residual stresses after completion of the weld are shown in Figure G.12. The outline of the buttering and weld are shown in this figure outlined in white. The stresses start as tensile near the inner radius, become compressive in the mid thickness region of the pipe, and return to tensile near the outer surface of the pipe. This behavior is quite typical for same material welds in thick pipe (Refs. G.6 and G.9). Axial residual stresses at the cold leg operating temperature of 291°C (556°F) are illustrated in Figure G.13. The main difference between the room temperature (Figure G.12) and operating residual stresses (Figure G.13) are magnitude.

The hoop residual stresses at room temperature and operating temperature are shown in Figures G.14 and G.15, respectively. Notice that hoop residual stresses remain tensile through out the entire pipe thickness in the region of the weld for both temperatures. Again, this is quite typical for same material (i.e., non bimetallic) welds in both thick and thin pipe (Refs. G.6 and G.9). Moreover, these higher hoop stresses and

Table G.1 Material properties for Inconel 182 weld material

T	C_p	λ	E	ν	σ_y	α
(°F)	(BTU/Lbm-F)	BTU/Sec-inch-F)	(ksi)		(ksi)	(10^{-6}/(°F))
70	0.095	0.00013	22674.70	0.3	38.50	6.50
200	0.110	0.000145	22023.96	0.3	36.18	6.73
400	0.120	0.000162	21022.83	0.3	33.55	7.09
600	0.125	0.000185	20021.70	0.3	30.00	7.44
800	0.130	0.000206	19051.70	0.3	28.26	7.62
1000	0.135	0.000226	18081.70	0.3	26.60	7.80
1200	0.140	0.000247	17987.40	0.3	26.20	8.10
1400	0.150	0.000273	17893.10	0.03	25.70	8.40
1600	0.160	0.000298	15621.95	0.3	19.03	8.70
1800	0.165	0.000324	13350.80	0.3	12.10	9.00
2000	0.170	0.000354	10000.00	0.3	3.70	9.20
2550	0.170	0.000354	200.00	0.3	0.40	9.20

T = Temperature ν = Poisson's constant
C_p = Specific heat σ_y = Yield stress
λ = Conductivity α = thermal expansion
E = Elastic Modulus

Table G.2 Temperature dependent material properties for A516-70

	C_p		λ	T	E	ν	σ_y	α
(°F)	(BTU/Lbm-F)	(°F)	BTU/Sec-inch-F)	(°F)	(ksi)		(ksi)	10^{-6}/(°F)
70	0.11	32	0.000694	72	31000.00	0.3	40.76	7.67
122	0.116	212	0.00067	300	29849.24	0.3	32.98	7.67
302	0.124	392	0.000647	550	28297.79	0.3	32.00	7.67
392	0.127	572	0.000617	700	26991.11	0.3	31.50	7.67
482	0.133	752	0.000571	932	25500.00	0.3	30.10	8.33
572	0.137	932	0.000527	1112	24300.00	0.3	23.70	8.33
662	0.143	1112	0.000476	1292	21000.00	0.3	15.90	8.61
842	0.158	1292	0.000425	1472	17000.00	0.3	8.00	8.61
1022	0.179	1472	0.000348	2732	203.00	0.3	0.44	8.89
1202	0.202	1832	0.000364					
1292	0.342	2192	0.000397					
1382	0.227							
1562	0.215							
1832	0.202							
2192	0.201							

T = Temperature ν = Poisson's constant
C_p = Specific heat σ_y = Yield stress
λ = Conductivity α = thermal expansion
E = Elastic Modulus

Table G.3 Temperature dependent material properties for A508 Class 3

C_p		λ		T	E	ν	σ_γ	α
(°F)	(BTU/Lbm-F)	(°F)	BTU/Sec-inch-F)	(°F)	(ksi)		(ksi)	10^{-6}/(°F)
70	0.11	32	0.000694	71.60	30784.93	0.3	54.52	7.67
122	0.116	212	0.00067	600.00	28807.05	0.3	43.78	7.67
302	0.124	392	0.000647	1000.00	25633.87	0.3	29.55	8.33
392	0.127	572	0.000617	1400.00	14540.00	0.3	9.78	8.61
482	0.133	752	0.000571	1800.00	10243.06	0.3	2.78	8.89
572	0.137	932	0.000527	2732.00	203.00	0.3	0.44	8.89
662	0.143	1112	0.000476					
842	0.158	1292	0.000425					
1022	0.179	1472	0.000348					
1202	0.202	1832	0.000364					
1292	0.342	2192	0.000397					
1382	0.227							
1562	0.215							
1832	0.202							
2192	0.201							

T = Temperature ν = Poisson's constant
C_p = Specific heat σ_γ = Yield stress
λ = Conductivity α = thermal expansion
E = Elastic Modulus

Table G.4 Temperature dependent material properties for Type 316 and Type 309

C_p		λ		T	E	ν	σ_γ	α
(°F)	(BTU/Lbm-F)	(°F)	BTU/Sec-inch-F)	(°F)	(ksi)		(ksi)	10^{-6}/(°F)
74.2	0.1079	70	0.000173	75	28400.00	0.30	38.00	8.09
165.4	0.1132	200	0.000186	300	27500.00	0.30	30.00	8.77
191.1	0.1143	400	0.000207	550	25950.00	0.30	23.40	9.33
399.6	0.1229	623	0.000231	700	24900.00	0.30	23.00	9.57
602.6	0.1291	800	0.000248	900	23500.00	0.30	22.00	9.84
794.4	0.132	1011	0.000269	1100	22200.00	0.30	20.50	10.09
1020.5	0.136	1195	0.000288	1300	20820.00	0.30	20.00	10.21
1203.7	0.1398	1391	0.000308	1500	19100.00	0.30	17.00	10.43
1409.6	0.145	1583	0.000327	1652	16900.00	0.30	14.10	10.60
1595.5	0.1505	1783	0.000348	1832	14500.00	0.30	8.46	10.70
1784.2	0.1556	1996	0.000369	2012	14500.00	0.30	3.77	10.90
1995.8	0.1622			2732	203.04	0.30	0.44	11.20

T = Temperature ν = Poisson's constant
C_p = Specific heat σ_γ = Yield stress
λ = Conductivity α = thermal expansion
E = Elastic Modulus

Table G.5 Temperature dependent material properties for Type 304

C_p		λ		T	E	ν	σ_y	α
(°F)	(BTU/Lbm-F)	(°F)	BTU/Sec-inch-F)	(°F)	(ksi)		(ksi)	10^{-6}/(°F)
74.2	0.1079	70	0.000173	75	28400.00	0.30	36.90	8.09
165.4	0.1132	200	0.000186	300	27500.00	0.30	27.70	8.77
191.1	0.1143	400	0.000207	550	25950.00	0.30	23.25	9.33
399.6	0.1229	623	0.000231	700	24900.00	0.30	21.80	9.57
602.6	0.1291	800	0.000248	900	23500.00	0.30	19.90	9.84
794.4	0.132	1011	0.000269	1100	22200.00	0.30	18.10	10.09
1020.5	0.136	1195	0.000288	1300	20820.00	0.30	16.20	10.21
1203.7	0.1398	1391	0.000308	1500	19100.00	0.30	11.40	10.43
1409.6	0.145	1583	0.000327	1652	16900.00	0.30	10.10	10.60
1595.5	0.1505	1783	0.000348	1832	14500.00	0.30	8.46	10.70
1784.2	0.1556	1996	0.000369	2012	14500.00	0.30	3.77	10.90
1995.8	0.1622			2732	203.04	0.30	0.44	11.20

T = Temperature
C_p = Specific heat
λ = Conductivity
E = Elastic Modulus

ν = Poisson's constant
σ_y = Yield stress
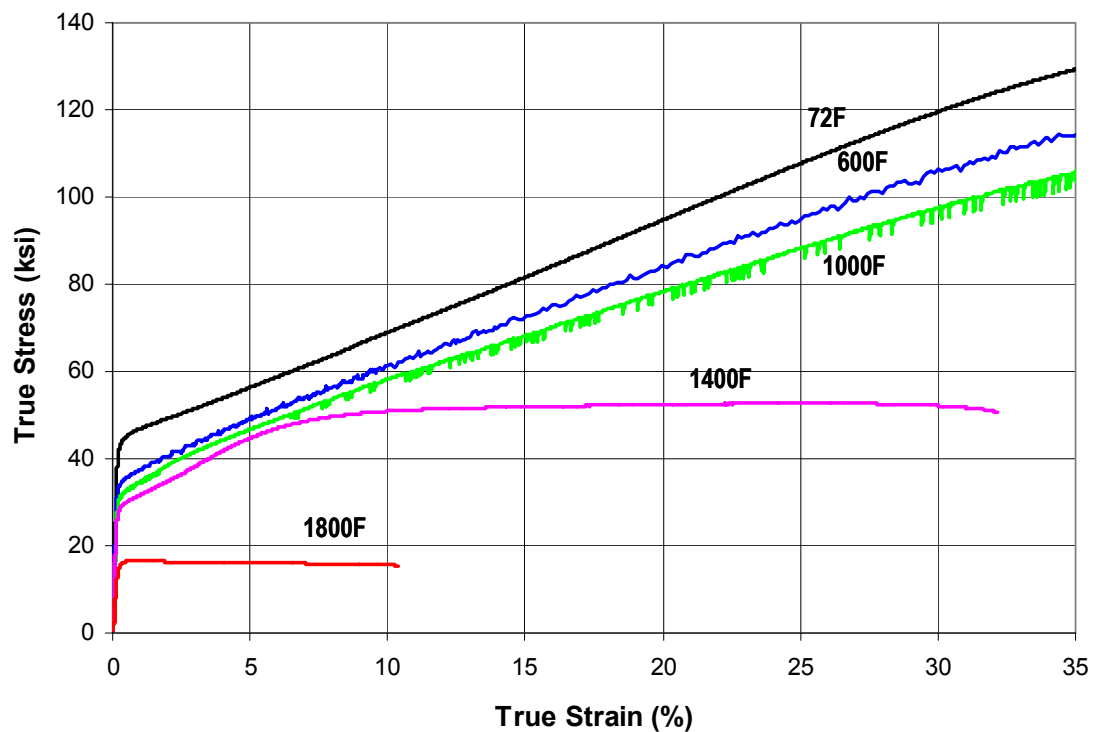α = thermal expansion

Figure G.7(a) Temperature dependent true stress-strain curves of Inconel 182 tested by ORNL